

Stability of g -modes in rotating B-type stars

Aprilia^{1*}, Umin Lee^{1†}, and Hideyuki Saio^{1‡}

¹*Astronomical Institute, Tohoku University, Sendai, Miyagi 980-8578, Japan*

Typeset 5 November 2018; Received / Accepted

ABSTRACT

We have studied the stability of low degree g -modes in uniformly rotating B-type stars, taking into account the effects of the Coriolis force and the rotational deformation. From an analysis treating rotation frequency as a small parameter it is found that slow rotation tends to *destabilize* high radial-order *retrograde* g -modes, although the effect is very small or absent for relatively low order modes. Calculating eigenfrequencies at selected rotation rates, we find, on the other hand, that rapid rotation tends to *stabilize retrograde* g -modes. The stabilizing effect appears stronger for less massive B-type stars having low effective temperatures. If we change rotation rate continuously, the frequency of a g -mode belonging to (ℓ, m) crosses frequencies of other g -modes belonging to (ℓ', m) . If the parity of the two encountering modes are the same, they interact each other and the stability (i.e., imaginary part of eigenfrequency) of each mode is modified. Using an asymptotic method we discuss the property of such mode crossings and couplings. For rapidly rotating stars mode couplings are important for the stability of low degree g -modes. In particular, we find that the stabilization of retrograde g -modes in rapidly rotating stars is due to many strong mode couplings, while *prograde sectoral* modes are exceptionally immune to the damping effects from the mode couplings.

Key words: stars: oscillations – stars : rotation

1 INTRODUCTION

The kappa-mechanism associated with the iron opacity bump at $T \sim 2 \times 10^5 \text{K}$ excites high-order g -modes in intermediate-mass ($7 \gtrsim M/M_\odot \gtrsim 3$) main-sequence stars (Gautschy & Saio 1993; Dziembowski, Moskalik, Pamyatnykh 1993). These B-type g -mode pulsators with typical periods of the order of days are called slowly pulsating B (SPB) stars, which Waelkens (1991) first recognized as an independent class of variables (see De Cat 2007, for a review). It is generally considered that majority of SPB stars are slow rotators with projected equatorial rotation velocities of $V \sin i \lesssim 100 \text{ km s}^{-1}$, although several SPB stars are known to have $V \sin i$ exceeding 200 km s^{-1} . However, the criterion for slow rotation may not be appropriate when we look into the effect of rotation on g -modes of SPB stars. For example, an equatorial rotation velocity of 50 km s^{-1} corresponds to an angular velocity $\Omega = 0.1 \sqrt{GM/R^3}$ if we adopt mass and radius typical for a SPB star; $M = 4M_\odot$ and radius, $R \approx 2.4R_\odot$, where G is the gravitational constant. This indicates that the centrifugal acceleration, $R\Omega^2$ is much

smaller than the surface gravity, GM/R^2 , causing negligible deformation of the structure of the star. However, the 50 km s^{-1} velocity corresponds to a rotation period of about 2.4 days, comparable to the typical pulsation periods of SPB stars; in other words, the ratio of rotation to pulsation frequency is comparable to unity. Since the Coriolis force affects stellar oscillations significantly when $2\Omega/\omega \gtrsim 1$ with ω being the oscillation frequency in the co-rotating frame (e.g., Unno et al. 1989), g -modes in most SPB stars might be affected significantly by the Coriolis force, even though rotational deformations are negligibly small.

In addition, it is known that g -modes are present in many rapidly rotating Be stars (e.g., Rivinius, Baade, & Štefl 2003). This is understandable because many Be stars are located in the SPB instability strip on the HR diagram. There is some evidence that the excitation of g -modes in Be stars should be affected significantly by rotation (e.g., Walker et al. 2005; Saio et al. 2007). Therefore, it is important to examine the effect of rotation on g -modes in B-type stars.

Stability analyses of g -modes in rotating B stars have been carried out by several authors (e.g., Lee 2001; Townsend 2005; Savonije 2005; Walker et al. 2005; Saio et al. 2007; Cameron et al. 2008). Lee (2001) calculated non-adiabatic g -modes of rotating SPB stars by taking into account the effect of the Coriolis force and found that the

* E-mail: aprilia@astr.tohoku.ac.jp

† E-mail: lee@astr.tohoku.ac.jp

‡ E-mail: saio@astr.tohoku.ac.jp

low degree unstable *retrograde* g -modes in the absence of rotation are stabilized by rapid rotation via mode couplings with high ℓ stable g -modes. Savonije (2005) obtained similar results on the stabilization of retrograde modes in rapidly rotating models, by solving a set of two dimensional partial differential equations describing small amplitude non-adiabatic oscillations of uniformly rotating stars. The tendency of retrograde modes being stabilized is more pronounced for g -modes in nearly critically rotating Be stars (Walker et al. 2005; Saio et al. 2007; Cameron et al. 2008).

On the other hand, such stabilization of retrograde modes does not occur if the traditional approximation is employed (Townsend 2005). The horizontal component of the angular velocity of rotation ($\Omega \sin \theta$ with θ being co-latitude) is neglected in the traditional approximation, which makes the set of the governing equations similar to the one without rotation. Only difference is that $\ell(\ell + 1)$ in the non-rotating case is replaced with λ_{km} (a function of $2\Omega/\omega$) in the traditional approximation, where $k = 0, 2, 4, \dots$ for even modes, while $k = 1, 3, 5, \dots$ for odd modes, in parallel to $\ell = |m| + k$ in the non-rotating case. The traditional approximation works well for g -modes except when two modes associated with the same m and parity (even or odd) but different λ_{km} s have similar frequencies; in the traditional approximation the two modes are independent, while the two modes couple in reality (Lee & Saio 1989). Therefore, the difference in the stability result based on the traditional approximation from the result without it can be explained by the absence of mode couplings under the traditional approximation. This indicates that mode couplings are important in the stability of g -modes in rotating stars. In this paper, we discuss the effect of the couplings on the stability of g -modes in detail.

2 METHOD OF CALCULATION

We use the method of calculation given in Lee & Baraffe (1995) to study the stability of g -modes in uniformly rotating stars by taking into account the effects of the Coriolis force and the centrifugal force. We employ a coordinate system (a, θ, ϕ) for a rotationally deformed star, where the coordinate a is regarded as the mean distance of equi-potential surface from the stellar centre. It is related to spherical polar coordinates (r, θ, ϕ) as

$$r = a [1 + \epsilon(a, \theta)], \quad (1)$$

where ϵ , a rotational deformation, can be written as

$$\epsilon = \alpha(a) + \beta(a)P_2(\cos \theta) \quad (2)$$

with the second Legendre polynomial $P_2(\cos \theta) = (3 \cos^2 \theta - 1)/2$. The term α represents the spherical expansion and β the deformation of the star due to rotation. Assuming that ϵ is proportional to Ω^2 , we calculate the functions $\alpha(a)$ and $\beta(a)$ by applying the Chandrasekhar-Milne expansion to the hydrostatic and Poisson equations for the star (see Lee & Baraffe 1995, for details).

We express the angular dependence of small amplitude oscillations of the star using finite series expansion in terms of spherical harmonic functions $Y_l^m(\theta, \phi)$. For a given azimuthal wavenumber m , the displacement vector $\xi(a, \theta, \phi, t)$ is given by

$$\frac{\xi_a}{a} = \sum_{j=1}^{j_{\max}} S_{l_j}(a) Y_{l_j}^m e^{i\omega t}, \quad (3)$$

$$\frac{\xi_\theta}{a} = \sum_{j=1}^{j_{\max}} \left[H_{l_j}(a) \frac{\partial}{\partial \theta} Y_{l_j}^m + T_{l'_j}(a) \frac{1}{\sin \theta} \frac{\partial}{\partial \phi} Y_{l'_j}^m \right] e^{i\omega t}, \quad (4)$$

$$\frac{\xi_\phi}{a} = \sum_{j=1}^{j_{\max}} \left[H_{l'_j}(a) \frac{1}{\sin \theta} \frac{\partial}{\partial \phi} Y_{l'_j}^m - T_{l_j}(a) \frac{\partial}{\partial \theta} Y_{l_j}^m \right] e^{i\omega t}, \quad (5)$$

and the Eulerian perturbation of the pressure, p' , for example, is given by

$$p'(a, \theta, \phi, t) = \sum_{j=1}^{j_{\max}} p'_{l_j}(a) Y_{l_j}^m(\theta, \phi) e^{i\omega t}, \quad (6)$$

where $\omega \equiv \sigma + m\Omega$ is the oscillation frequency in the co-rotating frame of the star with σ being the oscillation frequency in an inertial frame, and $l_j = |m| + 2(j - 1)$ and $l'_j = l_j + 1$ for even modes, and $l_j = |m| + 2j - 1$ and $l'_j = l_j - 1$ for odd modes, where $j = 1, 2, \dots, j_{\max}$, and j_{\max} is the length of the expansions. Note that the angular pattern of p' for even (odd) modes is symmetric (antisymmetric) with respect to the equator. Substituting these expansions into the linearized basic equations, we obtain a finite set of coupled first order linear ordinary differential equations for the expansion coefficients $S_{l_j}(a)$ and $p'_{l_j}(a)$, and for given values of the parameters m and Ω , we solve the set of the differential equations as an eigenvalue problem of ω by imposing appropriate boundary conditions at the centre and surface of the star. The set of the linear differential equations as well as the boundary conditions is given in Lee & Baraffe (1995). Since we assume that the perturbed quantities are proportional to $e^{i(m\phi + \omega t)}$, modes having negative ω_I are pulsationally unstable (or excited), where $\omega_I \equiv \text{Im}(\omega)$ and $\omega_R \equiv \text{Re}(\omega)$ denote respectively the imaginary part and the real part of ω . Note that when $\omega_R > 0$, modes associated with negative (positive) azimuthal wavenumber m are prograde (retrograde) modes seen in the co-rotating frame of the star.

To save computing time, we employ the Cowling approximation, neglecting the Eulerian perturbation of the gravitational potential. We ignore the effect of rotational spherical expansion of the equilibrium structure on the oscillation, that is, we set $\alpha = 0$ in equation (2), because it is just a change in mean radius not important for our qualitative study.

To determine an adequate length of the series expansions, j_{\max} , we have compared the results of sample calculations obtained with $j_{\max} = 6, 8, 10$, and 12. We have found that $j_{\max} = 10$ is large enough for unstable g -modes even for the case of rapid rotation $\Omega = 0.4 \sqrt{GM/R^3}$. Therefore, we have adopted $j_{\max} = 10$ in calculating eigenfrequencies and eigenfunctions of g -modes presented in this paper.

2.1 Mode identification and notation

As equations (3)–(6) indicate, the angular variation of a non-radial pulsation mode in a rotating star cannot be represented by a single spherical harmonic but need to be expanded into many harmonics for a given azimuthal order m . The angular variation of a mode depends on the ratio

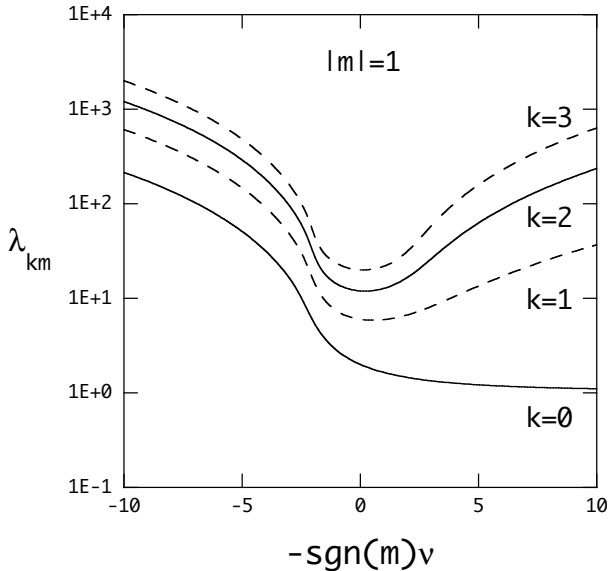


Figure 1. Eigenvalue of Laplace's tidal equation λ_{km} versus $-\text{sgn}(m)\nu$ for $|m| = 1$, where $\text{sgn}(m) \equiv m/|m|$ and $\nu \equiv 2\Omega/\omega$. Solid lines are for even modes and dashed lines for odd modes.

of rotation frequency to the oscillation frequency. To distinguish the angular dependence property of each mode, it is useful to refer to the mode properties under the traditional approximation, in which the term $-\Omega \sin \theta \mathbf{e}_\theta$ in $\mathbf{\Omega} = \Omega \cos \theta \mathbf{e}_r - \Omega \sin \theta \mathbf{e}_\theta$ is neglected. Many properties of low frequency oscillations of uniformly rotating stars are well explained by using the traditional approximation except for mode couplings (e.g., Lee & Saio 1987, 1997). In this approximation, the angular dependence of the oscillations are given by Hough function (e.g., Lindzen & Holton 1968) which is the eigenfunction, associated with the eigenvalue λ_{km} , of Laplace's tidal equation. For a given azimuthal wavenumber m , λ_{km} depends on the ratio $\nu \equiv 2\Omega/\omega$ and tends to $\ell(\ell+1)$ with $\ell = |m| + k$ as $\nu \rightarrow 0$ for $k \geq 0$. Fig. 1 shows λ_{km} as a function of ν for $k = 0-3$ with $|m| = 1$. The quantity $\sqrt{\lambda_{km}}$ represents a kind of surface wave number. Except for the prograde sectoral modes ($k = 0$), λ_{km} increases as the parameter ν increases. The prograde sectoral modes (associated with λ_{0m} ($m < 0$)) are special modes in rapidly rotating stars whose surface wavenumber is lower than the value at $\Omega = 0$, and hardly changes with Ω . We emphasize here that although we use the modal properties under the traditional approximation as guidelines to understand the behavior of g -modes as function of Ω , we do *not* use the traditional approximation in our numerical analyses.

To identify calculated modes, we make use of the fractional kinetic energy of oscillation mode defined as

$$f_j = e_j / \sum_{i=1}^{j_{\max}} e_i, \quad (7)$$

where

$$e_j = \int_0^R \left[|S_{l_j}|^2 + l_j(l_j+1) |H_{l_j}|^2 + l'_j(l'_j+1) |T_{l'_j}|^2 \right] 4\pi \rho a^4 da, \quad (8)$$

Table 1. Physical parameters of the main sequence models with $X = 0.7$ and $Z = 0.02$

Model	$M = 4M_\odot$			$M = 5M_\odot$		
	$\log \frac{L}{L_\odot}$	$\log T_{\text{eff}}$	X_c	$\log \frac{L}{L_\odot}$	$\log T_{\text{eff}}$	X_c
A	2.371	4.165	0.700	2.727	4.226	0.700
B	2.464	4.144	0.476	2.825	4.208	0.481
C	2.519	4.120	0.308	2.886	4.185	0.311
D	2.565	4.083	0.105	2.939	4.149	0.105

and $l_j = |m| + 2(j-1)$ and $l'_j = l_j + 1$ for even modes, and $l_j = |m| + 2j - 1$ and $l'_j = l_j - 1$ for odd modes.

If we find $f_j \geq 0.5$ with a particular value of j for a calculated *even* mode with a given m , we identify it as a mode associated with λ_{km} with $k = 2(j-1)$ (if the mode is an *odd* mode $k = 2j - 1$). For the case of rapid rotation, however, we sometimes need to use a somewhat relaxed criterion given by $f_j \geq \alpha$ with $\alpha < 0.5$, particularly for modes with $j > 1$. Also, we denote the mode as (ℓ, m) with $\ell \equiv |m| + k$ extending the familiar notation for nonradial pulsations of a non-rotating star. Note that prograde sectoral modes correspond to $\ell = -m$.

2.2 Unperturbed models

For unperturbed models of the stability analyses, we have calculated main-sequence evolution models without rotation, using a standard stellar evolution code using the OPAL opacity (Iglesias, Rogers & Wilson 1992; Iglesias & Rogers 1996). We have adopted masses of $4M_\odot$ and $5M_\odot$ with initial chemical compositions of $(X, Z) = (0.70, 0.02)$ as typical models for SPB stars. Table 1 shows parameters of selected models.

3 G-MODES EXCITED AT SELECTED ROTATION FREQUENCIES

Figs. 2-5 show growth rates, $\eta \equiv -\omega_I/\omega_R$, of unstable g -modes in the $4M_\odot$ and $5M_\odot$ ZAMS and D models (Tab. 1) at three selected rotation frequencies; $\bar{\Omega} = 0.01, 0.2$, and 0.4 , where $\bar{\Omega} \equiv \Omega/\sqrt{GM/R^3}$. The horizontal axes $-\text{sgn}(m)\bar{\omega}_R$ measure the oscillation frequency in the co-rotating frame of the prograde (retrograde) modes in positive (negative) direction, where $\bar{\omega} = \omega/\sqrt{GM/R^3}$. Cyan and red dots are for $(\ell, |m|) = (1, 1)$ and $(2, 1)$, respectively, while crosses and black dots are for $(\ell, |m|) = (2, 2)$ and $(3, 2)$, respectively.

Firstly let us look at the slowest rotation cases (left panels). When rotation is very slow, crosses and red dots are almost superposed on each other, because eigenfrequencies are independent of the azimuthal order m in a non-rotating star, and the first order rotational correction to the frequency, which is proportional to m , is small for slow rotation. The growth rates η as a functions of $\bar{\omega}_R$ are almost symmetric with respect to the axis of $\bar{\omega}_R = 0$. Many g -modes are excited in a certain frequency range depending on the effective temperature of each model; the unstable frequency range is lower for a lower effective temperature, which is obvious, for example, when a ZAMS case is compared to the case of the evolved D model. (We note that the density of g -modes

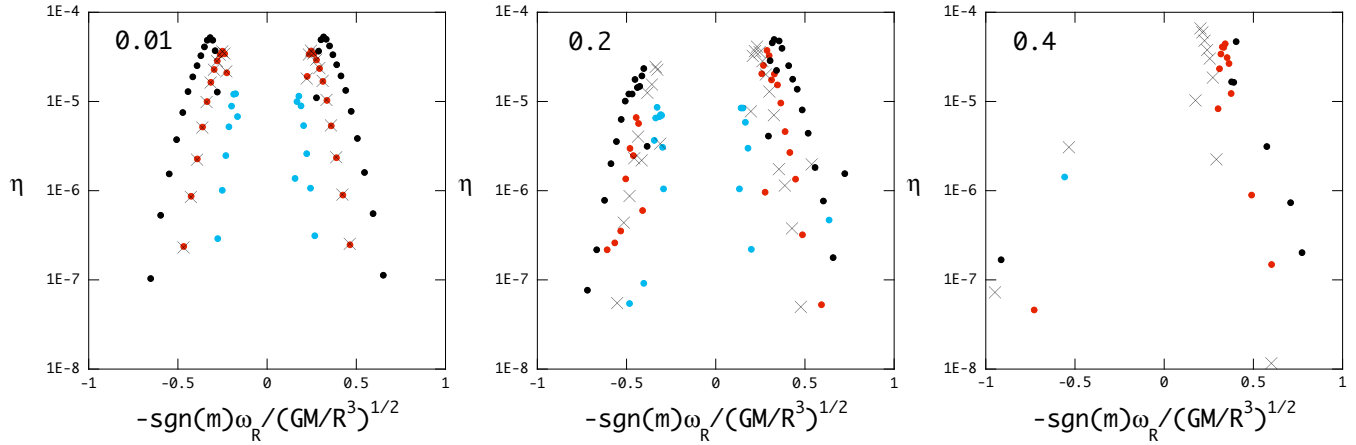


Figure 2. Growth rate $\eta \equiv -\omega_I/\omega_R$ versus $-\text{sgn}(m)\bar{\omega}_R$ for g -modes excited in the $4M_\odot$ ZAMS model A, where the cyan, red, and black dots stand for the g -modes with $(\ell, |m|) = (1, 1), (2, 1)$, and $(3, 2)$, respectively, and the crosses stand for the g -modes with $(\ell, |m|) = (2, 2)$. Left-, middle- and right-panels are for rotation frequencies of $\bar{\Omega} = 0.01, 0.2$ and 0.4 , respectively. Prograde modes having $m < 0$ appear on the right half of each panel, while retrograde modes ($m > 0$) appear on the left side.

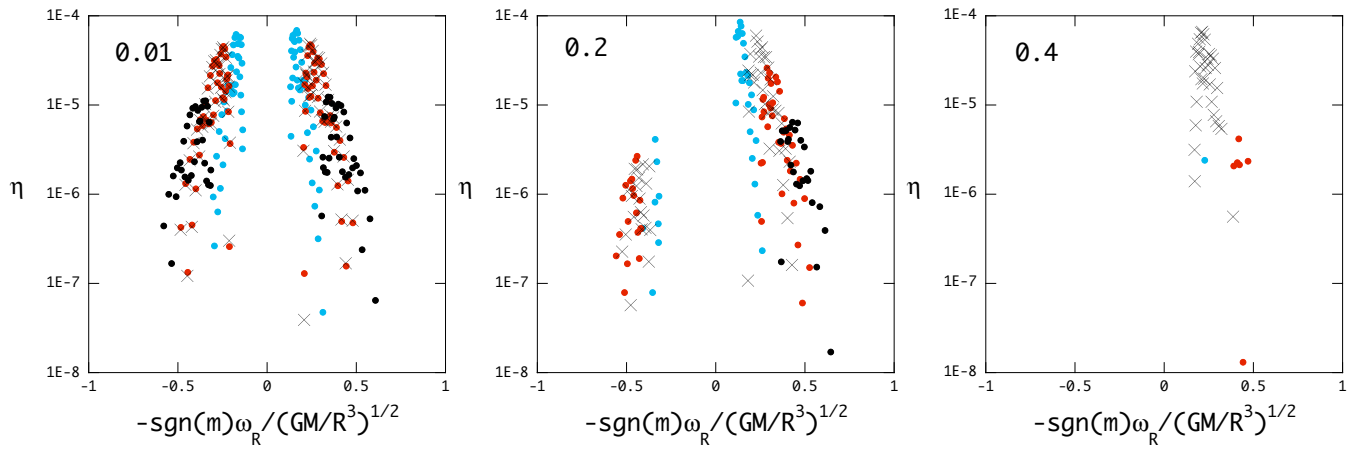


Figure 3. Same as Fig. 2 but for the $4M_\odot$ evolved main sequence model D.

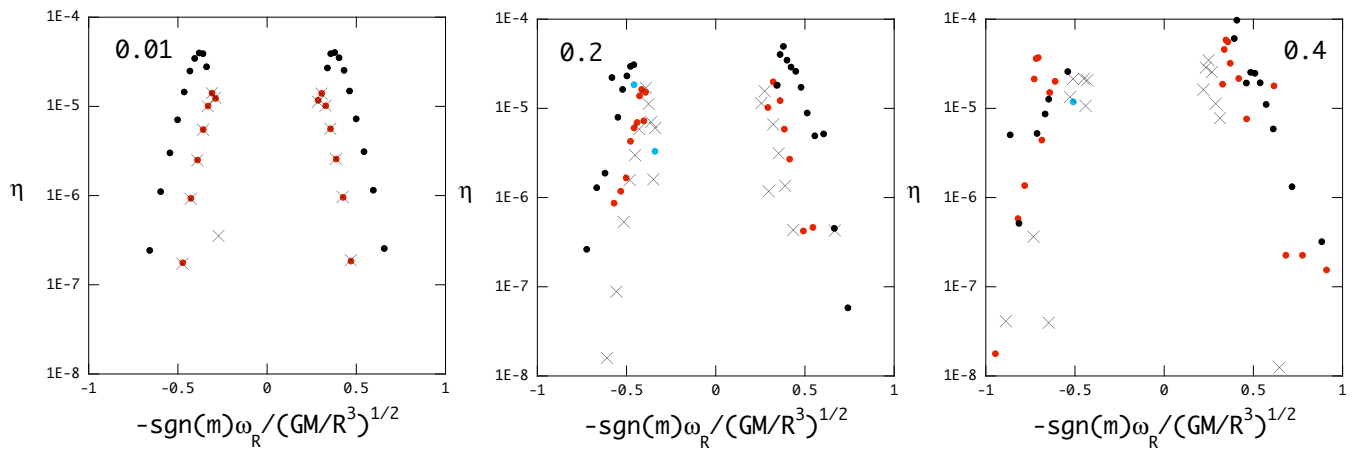


Figure 4. Same as Fig. 2 but for the $5M_\odot$ ZAMS model A.

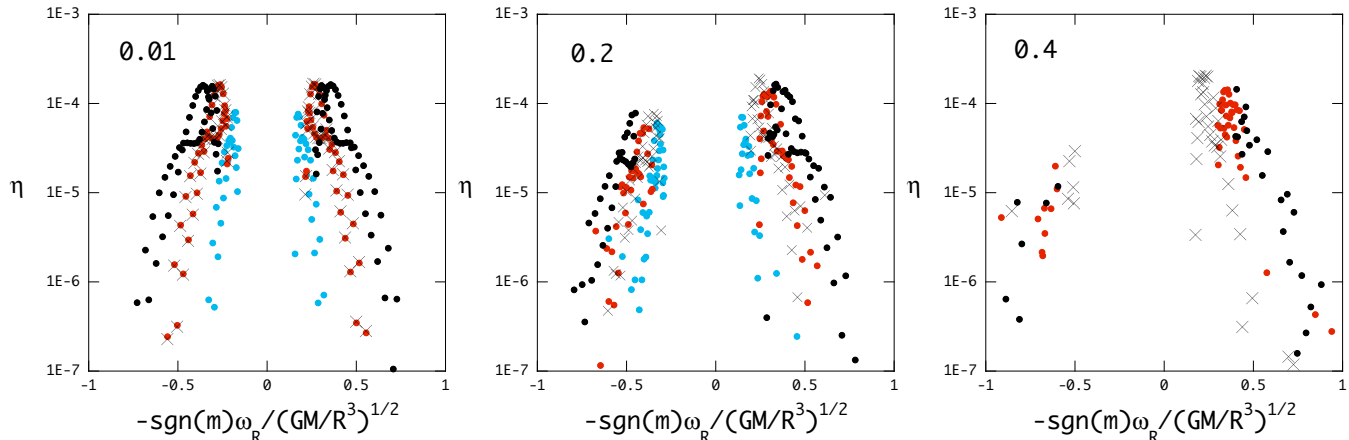


Figure 5. Same as Fig. 2 but for the evolved $5M_{\odot}$ main sequence model D.

is higher in the latter because the Brunt-Väisälä frequency increases as evolution proceeds.) This tendency of stability arises from the optimal condition for the kappa-mechanism of excitation; the kappa-mechanism is most effective when the thermal-timescale at the Fe opacity bump is comparable to pulsation periods (see e.g., Gautschy & Saio 1993). That is, longer-period modes tend to be excited in cooler models in which the opacity bump is located in deeper layers having longer thermal-times.

In the $5M_{\odot}$ ZAMS model (Fig. 4), $\ell = 1$ g -modes are not excited at $\bar{\Omega} = 0.01$, because their frequencies are too low to satisfy the optimal frequency condition for the kappa-mechanism. Retrograde $\ell = 1$ g -modes become unstable as the rotation frequency increases slightly as seen in the middle panel of Fig. 4. This is because the frequencies of retrograde modes have increased to enter into the frequency range where the kappa-mechanism works strongly enough to excite modes. Since the rotational effect on the frequency in a very slowly rotating star is approximately given as $mC_1\bar{\Omega}$ in the co-rotating frame with a positive constant C_1 (see the next section), frequencies of retrograde modes increase as the rotation rate increases.

It is seen in the panels for $\bar{\Omega} = 0.2$ and 0.4 in Figs. 2–5 that the prograde-retrograde symmetry is broken as the rotation frequency increases; the maximum growth rates for the retrograde modes become lower than those of the prograde modes, and the oscillation frequencies of the unstable retrograde modes increase as the rotation frequency increases, while the effect is not appreciable for the prograde modes. We also note that the number of unstable g -modes is largely reduced, particularly for the retrograde g -modes. This is due to selective damping caused by mode couplings, which will be discussed in §5.

Fig. 5 shows unstable g -modes of a $5M_{\odot}$ evolved main-sequence model, which has an effective temperature similar to that of the $4M_{\odot}$ ZAMS model (see Table 1). Comparing Fig. 5 with Fig. 2 for the $4M_{\odot}$ ZAMS model, we find that although the frequency spectra for the former model are much denser than those of the latter, rapid rotations stabilize retrograde modes similarly for both models. This may suggest that the stabilizing effect on retrograde g -modes mainly depends on the effective temperature, while the dif-

ference in the internal structure due to mass difference has only a minor effect.

Figs. 2–5 clearly show that in rapidly rotating stars *retrograde* modes tend to be stabilized more strongly than *prograde* modes. In particular, for the $4M_{\odot}$ evolved model shown in Fig. 3 only *prograde* (mostly sectoral $\ell = 2$) modes are excited. The retrograde–prograde mode asymmetry is less pronounced in relatively hotter models. This is (at least) partly because unstable frequency ranges in hotter models are higher (due to the optimal condition for the kappa-mechanism at the Fe opacity bump) so that the ratios $2\Omega/\omega$ (which govern the strength of the Coriolis force effect) for the excited modes are generally smaller, and hence the rotation effects are weaker in hotter models.

4 SLOW ROTATION

Let us next discuss the effect of slow rotation on the stability of g -modes in rotating B stars (e.g., Lee 2001). For oscillations in a slowly rotating star, we can treat the rotation frequency Ω as a small parameter, and express the oscillation frequency ω of a mode as

$$\bar{\omega}(\bar{\Omega}) = \bar{\omega}_0 + mC_1\bar{\Omega} + C_2\bar{\Omega}^2, \quad (9)$$

where ω_0 is the oscillation frequency of the mode in the absence of rotation. The coefficient C_1 represents the first order rotational effect due to the Coriolis force and the coefficient C_2 the second order effects that come from the centrifugal force and the Coriolis force. Since eigenfrequencies ω are complex numbers in nonadiabatic analyses, C_1 and C_2 are also complex numbers. The real part of C_1 , C_{1R} , is approximately equal to the adiabatic expression

$$C_{1R} \approx \frac{\int_0^R [2\xi_{ar}/\xi_{ah} + 1]\xi_{ah}^2 \rho r^2 dr}{\int_0^R [(\xi_{ar}/\xi_{ah})^2 + \ell(\ell+1)]\xi_{ah}^2 \rho r^2 dr} \quad (10)$$

(e.g., Unno et al. 1989), where subscript ‘a’ indicates adiabatic eigenfunctions.

We note that negative (positive) $C_{1I} = \text{Im}(C_1)$ means that the Coriolis force due to a slow rotation has destabilizing (stabilizing) effect on *retrograde* modes with $m > 0$ and stabilizing (destabilizing) effect on *prograde* modes with

$m < 0$, and that negative (positive) C_{2I} means the destabilizing (stabilizing) effect on both prograde and retrograde modes. In this paper, we have obtained the complex coefficients C_1 and C_2 for a given m , by computing the eigenfrequencies $\bar{\omega}$ of a mode at three different rotation frequencies, e.g., $\bar{\Omega} = 0, 10^{-3}$ and -10^{-3} , and substituting these values in equation (9). We confirmed that C_1 thus computed is in good agreement with that obtained with the method by Carroll & Hansen (1982).

In Fig. 6, we plot C_1 and C_2 versus $\bar{\omega}_R$ for $\ell = |m| = 1$ g -modes of $4M_\odot$ main sequence models, of which physical parameters are tabulated in Table 1. For the ZAMS model C_1 and C_2 are essentially the same as the result of Lee (2001). The coefficients C_{1R} for the evolved models are systematically larger than that for the ZAMS model. This can be understood as follows. In the interior of an evolved model the Brunt-Väisälä frequency N is higher than in the ZAMS model. An asymptotic theory of nonradial pulsations (e.g., Shibahashi 1979) gives the ratio of radial to horizontal displacement as $|\xi_r/\xi_h| \sim \sqrt{l(l+1)}|\omega/N|$, which indicates the ratio $|\xi_r/\xi_h|$ is smaller in the evolved models. The smaller ratio, in turn, yields larger C_{1R} as seen from equation (10).

In addition, C_{1R} for an evolved model has many regularly spaced peaks. The peaky features are also found in the imaginary parts of C_1 and C_2 for the evolved models. We have also calculated C_1 and C_2 for $10M_\odot$ main sequence models (not shown) to find quite similar behavior of the coefficients as functions of $\bar{\omega}_R$. The peaks in C_1 are caused by g -mode eigenfunctions being trapped in the μ -gradient zone (μ stands for mean molecular weight) above the convective-core boundary, in which the Brunt-Väisälä frequency is much higher than the adjacent layers. As discussed above, this yields larger C_{1R} for the trapped modes.

The regularity of the peaks is also understood from the asymptotic theory, which gives the frequency of a g -mode trapped in the μ -gradient zone, ω_μ , as

$$\omega_\mu \approx \frac{\sqrt{l(l+1)}}{n_\mu \pi} \int_{\Delta r} \frac{N}{r} dr, \quad (11)$$

where Δr and n_μ denote respectively the width of the μ -gradient zone and the number of radial nodes within the zone. Equation (11) indicates that the frequency separation between two consecutive trapped g -modes is proportional to $[n_\mu(n_\mu + 1)]^{-1}$, which explains why peaks are regularly spaced and the separations of peaks decrease with increasing radial orders (or decreasing frequencies).

The imaginary parts of C_1 and C_2 decrease rapidly as $\bar{\omega}_R$ decreases in the range $\bar{\omega}_R \lesssim 0.3$. Since the imaginary part of C_1 is negative for high radial-order g -modes, slow rotation has *destabilizing* (stabilizing) effect on high radial-order *retrograde* (prograde) g -modes. Considering that the imaginary part of C_2 is also negative for the high radial-order g -modes, the destabilizing effect of slow rotation on the g -modes works more strongly for the high radial-order retrograde modes. For relatively low radial-order modes both C_{1I} and C_{2I} are very small, indicating a slow rotation affects little the stability of these modes. The steep decreases of the imaginary parts of C_1 and C_2 with decreasing g -mode frequencies can be understood from the relation between the period of a high order g -mode and the optimal period for the kappa-mechanism excitation that is roughly the thermal timescale

at the Fe opacity bump. The period of a very high-order g -mode that has negative C_{1I} and C_{2I} is much longer than the optimal period for the kappa-mechanism. If the mode is a retrograde mode, both the first order and the second order effects of rotation increase the frequency (or decrease the period) as eq.(9) indicates. This effect makes the kappa-mechanism to work stronger to the mode, and appears as negative C_{1I} and C_{2I} ; in other words, the first and the second order rotation effects tend to destabilize very high-order retrograde g -modes. On the other hand, for a prograde mode the first order effect increases the period, while the second order effect decreases the period. Therefore, the first order rotation effect tends to stabilize a prograde mode, while the second order effect tends to destabilize it.

5 MODE COUPLINGS

5.1 Numerical Results

Fig. 7 shows the complex frequencies $\bar{\omega}$ of selected even g -modes of $(\ell, |m|) = (1, 1)$ (associated with $\lambda_{0\pm 1}$) (red lines) and of $(\ell, |m|) = (3, 1)$ (associated with $\lambda_{2\pm 1}$) (black lines) as functions of $\bar{\Omega}$ for the $4M_\odot$ ZAMS model, where the radial orders of the g -modes range from 21 to 26 for the $\ell = 3$ modes and from 9 to 11 for the $\ell = 1$ modes. The left panels, (a) and (b), are for prograde ($m = -1$) modes, while the right panels, (c) and (d), are for retrograde ($m = +1$) modes.

The variation of pulsation frequency ω_R of a g -mode as a function of Ω reflects the variation of λ_{km} as a function of ν . For a high order g -mode, pulsation frequency is approximately written as

$$\bar{\omega}_R \approx \frac{\sqrt{\lambda_{km}}}{n\pi} \int_0^1 \bar{N} \frac{dx}{x}, \quad (12)$$

where n is the radial order, $\bar{N} \equiv N/\sqrt{GM/R^3}$ normalized Brunt-Väisälä frequency, and x fractional radius r/R (Lee & Saio 1987, 1989). The equation indicates that the frequency of a prograde sectoral mode ($\ell = -m = 1$) slightly decreases but stays nearly constant as the rotation frequency increases just as λ_{0-1} behaves as a function of ν . The frequencies of the other modes in Fig. 7 increase at different rates depending on the corresponding λ_{km} s. Therefore, the oscillation frequency of a g -mode associated with a given λ_{km} crosses with another g -mode associated with $\lambda_{k'm}$ ($k' \neq k$) as seen in Fig. 7.

For adiabatic modes having real frequencies, a mode crossing between g -modes leads to an avoided crossing, but for non-adiabatic modes having complex frequencies, mode crossing is not always an avoided one. More importantly, a mode crossing between non-adiabatic g -modes can change the stability of the modes. The imaginary parts of eigenfrequencies as functions of Ω in Fig. 7 show numerous narrow peaks large and small. We consider that these peaks are caused by mode couplings. In panel (d) of Fig. 7 we recognize two pairs of a small peak and dip around $\bar{\Omega} \sim 0.06$ and ~ 0.07 , while panel (c) shows that a black line crosses a red line at each of the same $\bar{\Omega}$, indicating these peaks and dips in ω_I are caused by mode crossings. Large peaks in ω_I can be interpreted as couplings with strongly damped modes associated with higher radial orders and higher $\lambda_{k'm}$ having $k' = 2, 4, \dots$.

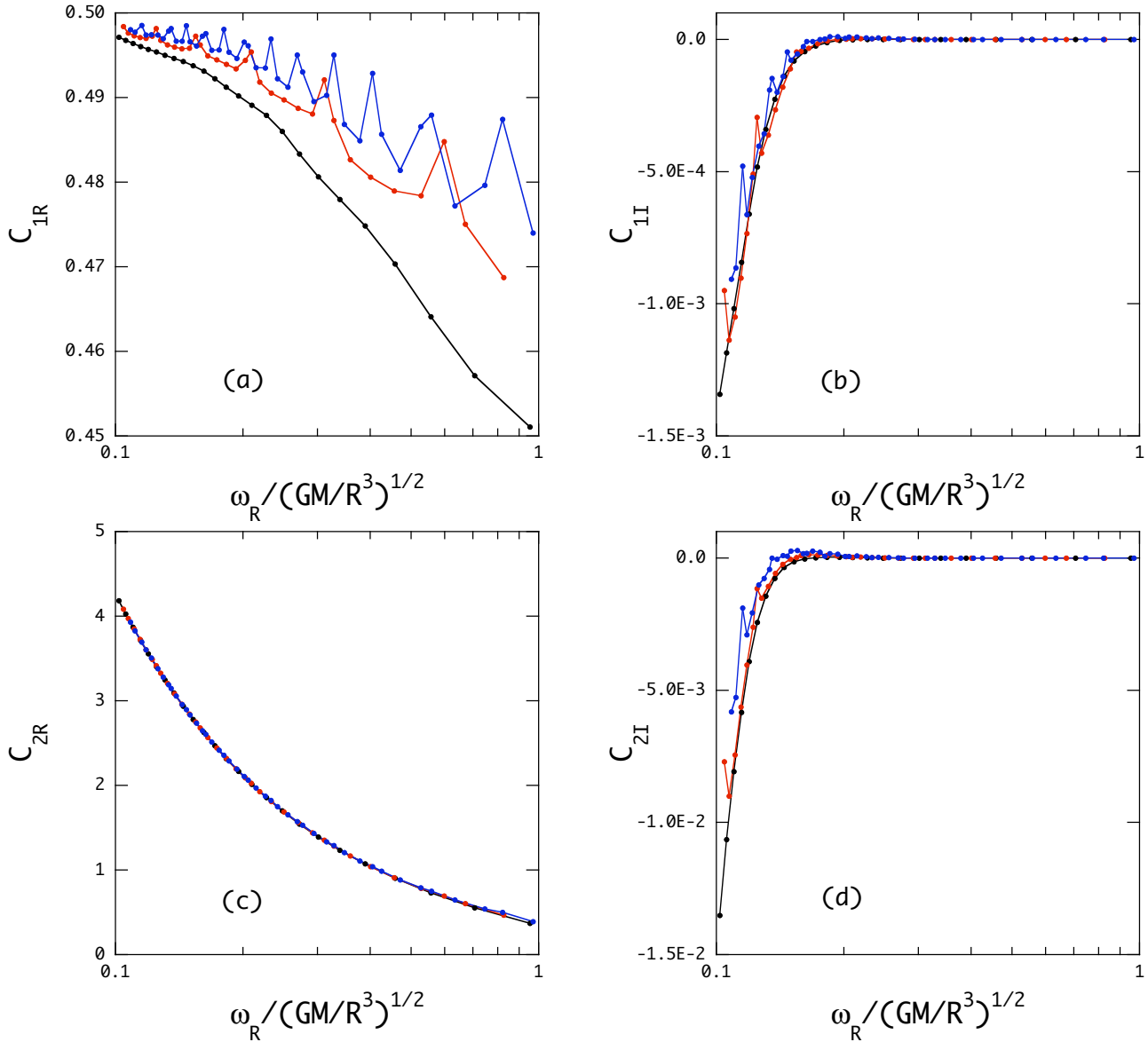


Figure 6. Complex coefficients C_1 and C_2 versus $\bar{\omega}_R$ for $\ell = |m| = 1$ g -modes of the $4M_\odot$ main sequence models, where the black, red, and blue lines indicate, respectively, the models A (ZAMS), B, and C in Table 1.

Since $|\bar{\omega}_I|$ of the $\ell = 1$ ($\lambda_{0\pm 1}$) g -modes is much smaller than that of the $\ell = 3$ ($\lambda_{2\pm 1}$) g -modes, zoomed diagrams of the former case are given in Fig. 8. For the $\ell = 1$ retrograde modes (panel (b)) $\bar{\omega}_I$ behaves similarly to $\ell \geq 3$ cases with numerous high peaks. This is reasonable because the frequency $\bar{\omega}_R$ of a retrograde $\ell = 1$ mode increase with $\bar{\Omega}$ similarly to the modes of $\ell \geq 3$ so that similar mode couplings would occur. On the other hand, the stability of *prograde* $\ell = 1$ (λ_{0-1}) modes behaves differently; for $\bar{\Omega} \gtrsim 0.2$, sharp peaks are replaced with broad bumps which become weak as $\bar{\Omega}$ increases, and those unstable modes stay unstable even at large $\bar{\Omega}$. This property is common for prograde sectoral modes and consistent with the results in Figs. 2 and 3 which show prograde sectoral modes being excited even at a rapid rotation.

Let us now look into two crossings which occur between modes of $(\ell, m) = (1, 1)$ and $(3, 1)$ (or between λ_{01} and λ_{21})

in detail. Fig. 9 shows a zoomed diagram around a crossing at $\bar{\Omega} \approx 0.06$ which is recognized as connected small peak and dip in Fig. 7 (panel d). The crossing occurs between the modes g_9 of $(\ell, m) = (1, 1)$ (red line) and g_{22} of $(\ell, m) = (3, 1)$ (black line). As this figure shows, the real parts of the eigenfrequencies make an avoided crossing, while the imaginary parts make a true crossing. At the crossing the properties of the modes are interchanged.

Fig. 10 shows another example of mode crossings which occurs between g_{10} -mode of $(\ell, m) = (1, 1)$ (red line) and g_{25} -mode of $(\ell, m) = (3, 1)$ (black line) at $\bar{\Omega} \approx 0.026$. The real parts of the frequencies appear to make a true crossing, while the imaginary parts show only a very small dip and bump. This crossing may be understood as a crossing with an interaction much weaker than the case of Fig. 9. The weak interaction reduces the distance at the closest encounter of

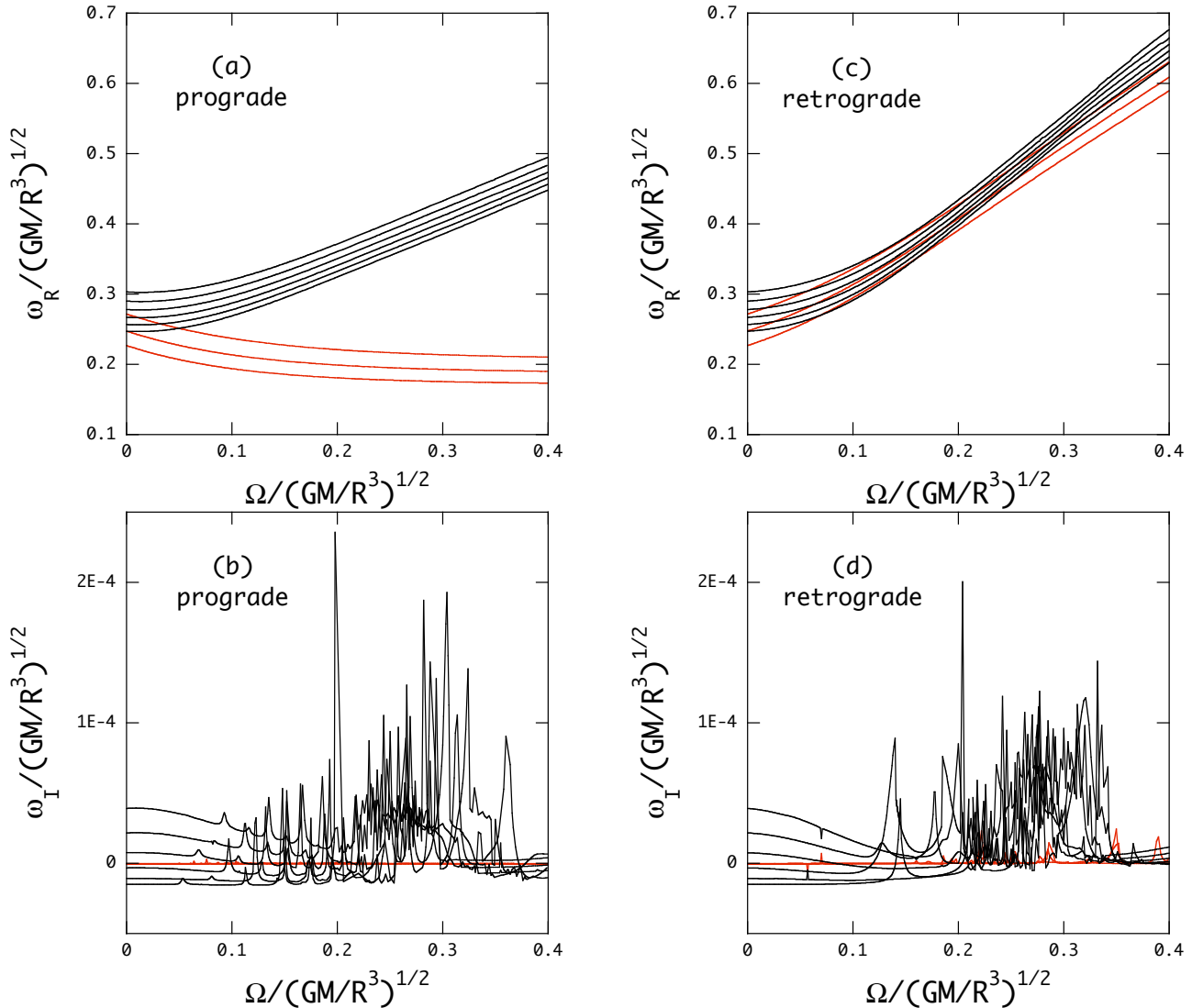


Figure 7. Complex $\bar{\omega}$ of even $|m| = 1$ g -modes of the $4M_{\odot}$ ZAMS model as functions of $\bar{\Omega}$ for prograde modes in panels (a) and (b) and for retrograde modes in panels (c) and (d), where the red curves denote the even $\ell = 1$ g -modes and the black curves the even $\ell = 3$ g -modes. Here, the radial order of the g -modes ranges from 9 to 11 for $\ell = 1$ and from 21 to 26 for $\ell = 3$.

ω_{RS} to zero and causes only very small effects on the stability of the modes.

5.2 Asymptotic Analysis

5.2.1 Coupling coefficient

It is helpful to discuss the mode crossing phenomena by using an asymptotic method based on the traditional approximation. Under the traditional approximation, the oscillation modes of a rotating star are separated into independent modes associated with different λ_{km} s. The traditional approximation works well for g -modes except when the frequencies of two modes with the same m and the same (even or odd) parity become very close to each other. Under the traditional approximation these two modes are independent, but in reality the term $-\Omega \sin \theta \mathbf{e}_{\theta}$, neglected in the approximation, brings about mode coupling between them.

Here, we extend the asymptotic analysis for adiabatic

oscillations developed by Lee & Saio (1989) to the case of non-adiabatic oscillations. Note that no effects of the centrifugal force are included in the following asymptotic treatment, and only the effects of the Coriolis force are considered. Lee & Saio (1989) have derived a dispersion relation which should be satisfied by adiabatic g -modes associated with λ_{jm} and λ_{km} ;

$$\tan \Psi_j \tan \Psi_k = \epsilon_{jk}, \quad (13)$$

where

$$\Psi_j = - \int_{x_c}^1 k_j dx + \frac{n_e}{2} \pi, \quad (14)$$

x_c denotes the outer boundary of the convective core, n_e is the effective polytropic index at the surface, and

$$k_j = \frac{\sqrt{\lambda_{jm}} \bar{N}}{x \bar{\omega}}. \quad (15)$$

The right hand side of equation (13), ϵ_{jk} , represents the

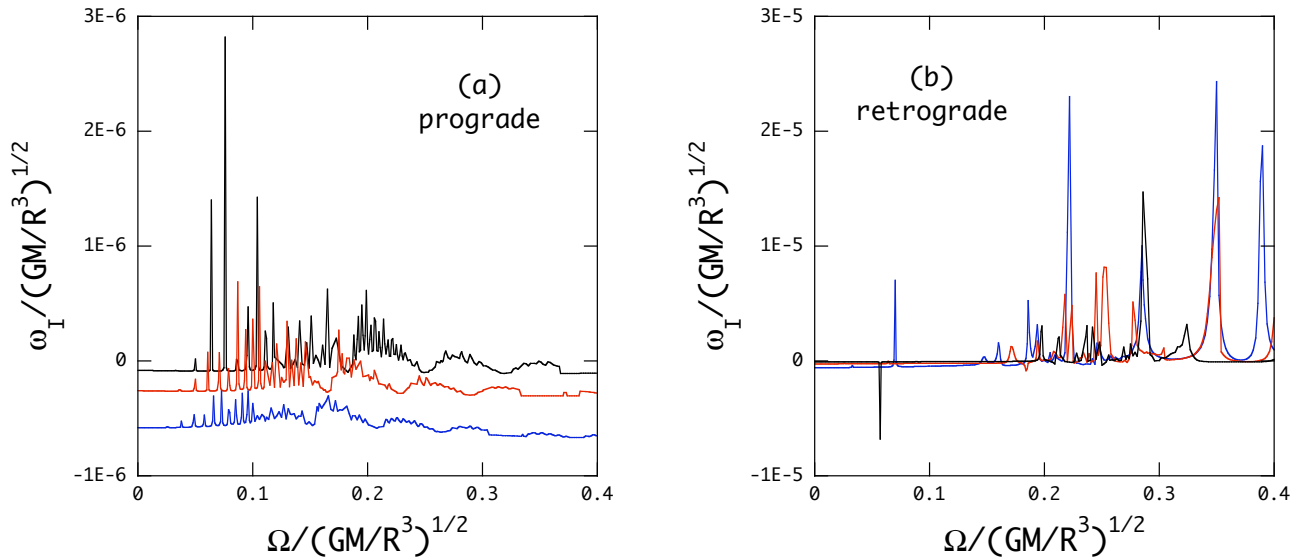


Figure 8. Zoomed diagrams for $\bar{\omega}_I$ of even $\ell = |m| = 1$ g -modes of the $4M_\odot$ ZAMS model as functions of $\bar{\Omega}$ for prograde modes in panel (a) and for retrograde modes in panel (b), where the black, red, and blue curves denote the g_9 , g_{10} , and g_{11} -modes, respectively.

effect of coupling between the two g -modes. We call it “coupling coefficient”. Note that if the coupling were absent (i.e., $\epsilon_{jk} = 0$), equation (13) would be reduced to $\tan \Psi_j = 0$ and $\tan \Psi_k = 0$, which give essentially the same expressions for $\bar{\omega}_j$ and $\bar{\omega}_k$ as equation (12).

The coupling coefficient ϵ_{jk} arises from a deviation from the traditional approximation around a crossing between g -modes associated with λ_{jm} and λ_{km} . Lee & Saio (1989) derived the expression

$$\epsilon_{jk} = \left[\int_{x_c}^1 \frac{dx}{x} \left(\left| \frac{\lambda_{jm}}{\lambda_{km}} \right|^{1/4} G_{jk} \cos \chi^j \sin \chi^k + \left| \frac{\lambda_{km}}{\lambda_{jm}} \right|^{1/4} G_{kj} \cos \chi^k \sin \chi^j \right) \right]^2, \quad (16)$$

where

$$\chi^j = - \int_{x_c}^x k_j dx + \frac{n_e}{2} \pi \quad (17)$$

and G_{jk} is a matrix element defined in Lee & Saio (1989), which consists of terms conflicting with the traditional approximation and brings about coupling between the two modes. The matrix element G_{jk} is proportional to ν so that $\epsilon_{jk} \rightarrow 0$ as $\nu \rightarrow 0$. This corresponds to the fact that modes with different ℓ s are independent in a non-rotating star.

From equation (16), we can calculate ϵ_{jk} as a function of ν (or $\bar{\omega}$) for given m , Ω , and (j, k) . However, only discrete values of ν satisfy the dispersion relation in equation (13). We obtained frequencies satisfying the dispersion relation by solving equation (13) numerically with Newton’s method in the frequency range between $\bar{\omega} = 0.1$ and $\bar{\omega} = 1$ for the $4M_\odot$ ZAMS model. The values of ϵ_{jk} at the discrete frequencies thus obtained are shown in Fig. 11 for $(j, k) = (0, 2)$, and in Fig. 12 for $(j, k) = (0, 4)$ and $(2, 4)$. Each point corresponds to a g -mode belonging to $\lambda_{j,m}$ or $\lambda_{k,m}$. Since $\lambda_{j,m}$ (and/or $\lambda_{k,m}$) increases rapidly with ν (except for the case of λ_{0m} with $m < 0$; Fig. 1), a large number of g -mode frequencies enter into the range $0.1 \leq \bar{\omega} \leq 1$ (cf. eq. 12).

Fig. 11 shows the coupling coefficient ϵ_{jk} between even g -modes associated with λ_{0m} ($\ell = |m|$) and λ_{2m} ($\ell = |m| + 2$) for $|m| = 1$ (panel a) and $|m| = 2$ (panel b) as functions of ν . The coupling coefficients increase rapidly as the parameter ν increases, which is reasonable because without rotation two modes with different ℓ s are independent from each other. For prograde ($m < 0$) modes, the coefficients level off for $\nu \gtrsim 2$ so that the coupling coefficients of prograde modes are appreciably smaller than those of retrograde modes when ν is sufficiently large.

Figure 12, shows coupling coefficients between g -modes associated with $\lambda_{0\pm 1}$ ($\ell = 1$) and $\lambda_{4\pm 1}$ ($\ell = 5$) in panel (a), and between those associated with λ_{2m} ($\ell = 3$) and λ_{4m} ($\ell = 5$) in panel (b). Obviously, the latter is much larger than the former at a given ν .

Fig. 11a shows that coupling coefficients are larger if $\bar{\Omega} = 0.4$ (red dots) is used rather than 0.2 (black dots), indicating coupling is stronger in a rapid rotator for a given value of ν .

We also found that the coupling coefficients for the $5M_\odot$ ZAMS model (not shown) are similar to those of $4M_\odot$ ZAMS model shown in the figures.

5.2.2 Quasi-adiabatic extension

In order to study mode couplings between nonadiabatic g -modes with the dispersion relation, it is necessary to extend it by including non-adiabatic effects. We modify the wavenumber k_j in the quasi-adiabatic approximation as

$$k_j = \frac{\sqrt{\lambda_{jm}} \bar{N}}{x} \frac{1}{\bar{\omega}} \sqrt{1 + i\beta_j \frac{\delta_T (\nabla_{ad} - \nabla)}{\delta_T (\nabla_{ad} - \nabla) + \nabla_\mu}} \quad (18)$$

(Lee 1985), where the oscillation frequency $\bar{\omega}$ is now regarded as a complex number, and

$$\beta_j = \lambda_{jm} \frac{\bar{N}^2}{\bar{\omega}^2} \frac{1}{\bar{\omega} c_2 V \nabla}, \quad c_2 = \frac{4\pi r^3 \rho T c_p}{L_r} \sqrt{\frac{GM}{R^3}}, \quad (19)$$

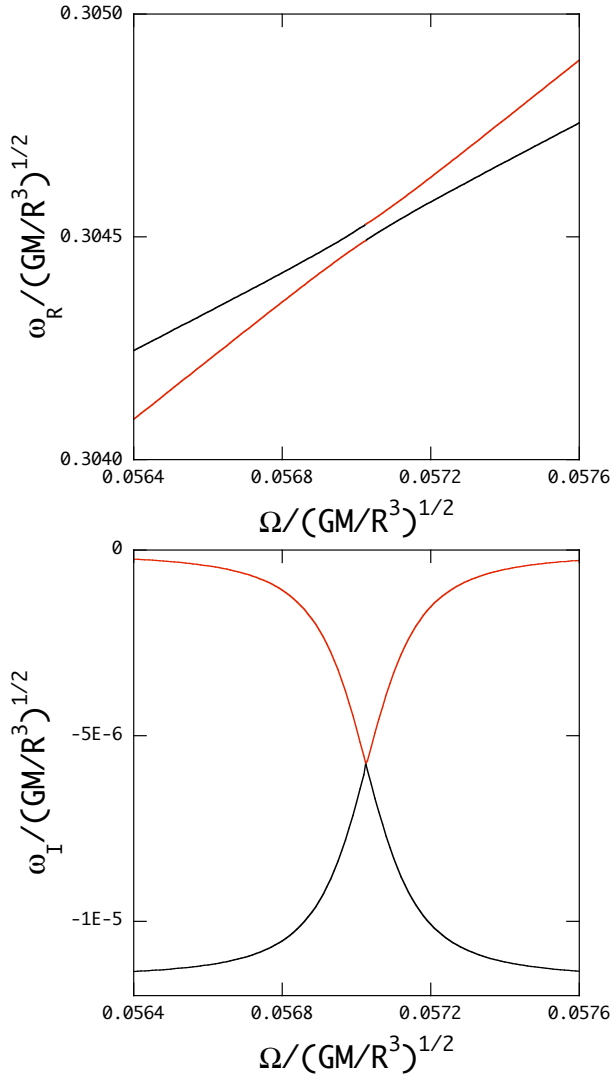


Figure 9. Mode crossing between $\ell = m = 1$ g_9 mode (red line) and $\ell = 3, m = 1$ g_{22} mode (black line). The real part makes an avoided crossing, where the mode property is exchanged at the closest approach.

$\delta_T = -(\partial \ln \rho / \partial \ln T)_p$, $\nabla_{\text{ad}} = (\partial \ln T / \partial \ln p)_{\text{ad}}$, $\nabla = d \ln T / d \ln p$, $\nabla_\mu = d \ln \mu / d \ln p$, $V = -d \ln p / d \ln r$, and L_r is the radiative luminosity and c_p is the specific heat at constant pressure. Here, for simplicity we have considered only radiative damping as the non-adiabatic effect. We note that if we define the local thermal time scale τ_{th} as $\tau_{\text{th}} = 4\pi r^2 H_p \rho T c_p / L_r$ with $H_p = -dr / d \ln p$ being the pressure scale-height, we have $\bar{\omega} c_2 / V = 2\pi \tau_{\text{th}} / P$ with $P = 2\pi / \omega$ being the oscillation period, and the term containing β_j , which represents the radiative damping effect, is proportional to P / τ_{th} . For the quasi-adiabatic approximation to be valid, we take account of the non-adiabatic contribution only in the region where $P / \tau_{\text{th}} \lesssim 0.01$. This criterion, however, is somewhat ambiguous since we ignore destabilizing contributions near the surface where $P / \tau_{\text{th}} \sim 1$.

Replacing the radial wavenumber in equation (15) by the complex wavenumber given in equation (18), we solve the dispersion relation in equation (13) to obtain complex frequencies $\bar{\omega}$ as functions of $\bar{\Omega}$, where we use $n_e = 3.525$.

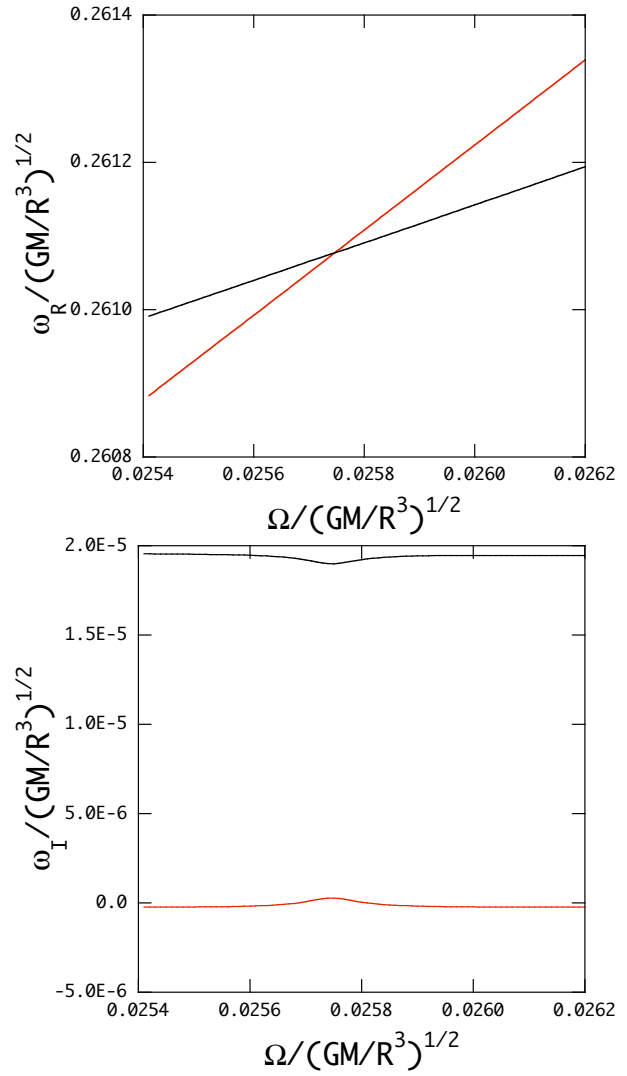


Figure 10. Mode crossing between $(\ell, m) = (1, 1)$ g_{10} (red line) and $(\ell, m) = (3, 1)$ g_{25} (black line) modes.

Note that since we include only radiative damping as the non-adiabatic contribution, we obtain only stable modes having positive ω_I .

Figs. 13–15 show three examples of mode crossings calculated using the dispersion relation in equation (13). Fig. 13 corresponds to the mode crossing in Fig. 9, in which the real parts of the eigenfrequencies make an avoided crossing and the imaginary parts make a true crossing causing a large peak and dip. Fig. 14 corresponds to that in Fig. 10, in which the real parts of the eigenfrequencies appear to make a true crossing and the imaginary parts show a small dip and bump. The coupling coefficient ϵ_{jk} for the case of Fig. 13 is of the order of 10^{-4} , while for the case of Fig. 14 it is of the order of 10^{-6} , supporting the previous conjecture that a weak interaction leads to such a crossing as seen in Fig. 10. The value of $\bar{\Omega}$ at which the mode crossing takes place does not necessarily agree well between the asymptotic method and the pulsation calculation. A possible reason for the disagreement may be attributable to neglecting the effect of the centrifugal force in the asymptotic treatment. The derivatives $d\omega_R / d\Omega$ for low frequency g -modes are different between the

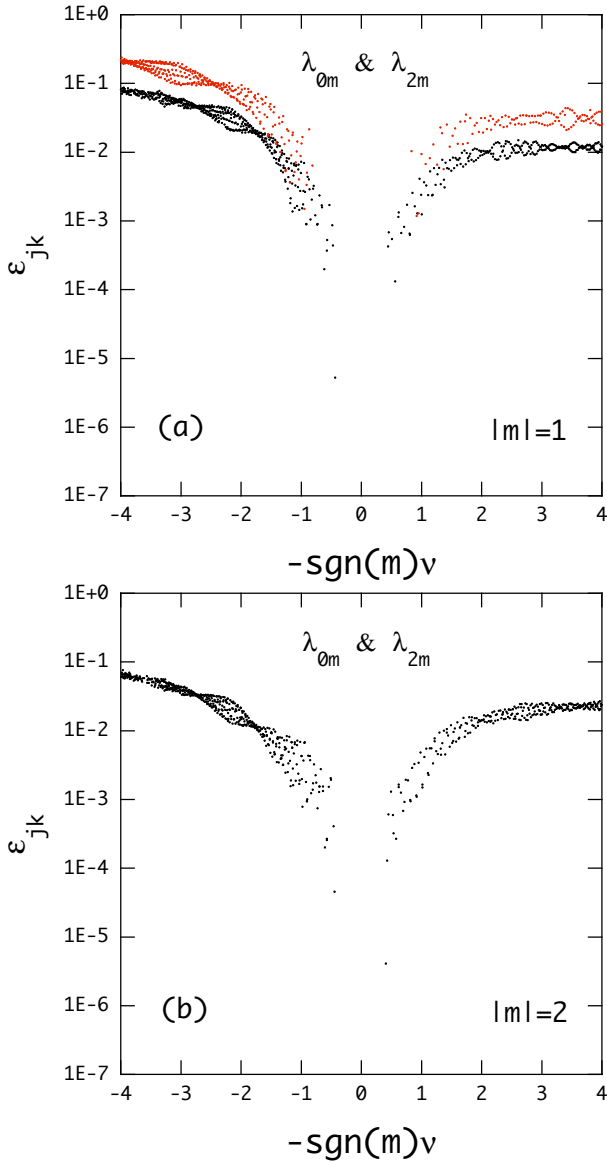


Figure 11. Coupling coefficient ϵ_{jk} between even g -modes associated with λ_{0m} and λ_{2m} for $|m| = 1$ in panel (a) and for $|m| = 2$ in panel (b) as a function of $\nu = 2\Omega/\omega$. Here, we have used the $4M_{\odot}$ ZAMS model, and assuming $\bar{\Omega} = 0.2$ (black dots) and $\bar{\Omega} = 0.4$ (red dots) we have calculated g -modes in the frequency range between $\bar{\omega} = 0.1$ and 1.

cases with and without the effects of the centrifugal force on the modes, and a slight difference in the derivatives may cause a large difference in the locations of g -mode crossing between the two cases having similar gradients $d\omega_R/d\Omega$.

Fig. 15 shows a mode crossing between two g -modes associated with λ_{2m} and λ_{4m} for $m = 1$ which has a broad interaction range in $\bar{\Omega}$. The broad interaction is possible if the oscillation frequencies of the two modes have similar dependence on the rotation frequency (i.e., similar $d\omega_R/d\Omega$) around the crossing, and the coupling coefficient is sufficiently large. The latter requirement is obviously met for the crossings between λ_{2m} and λ_{4m} g -modes (see panel (b) of Fig. 12).

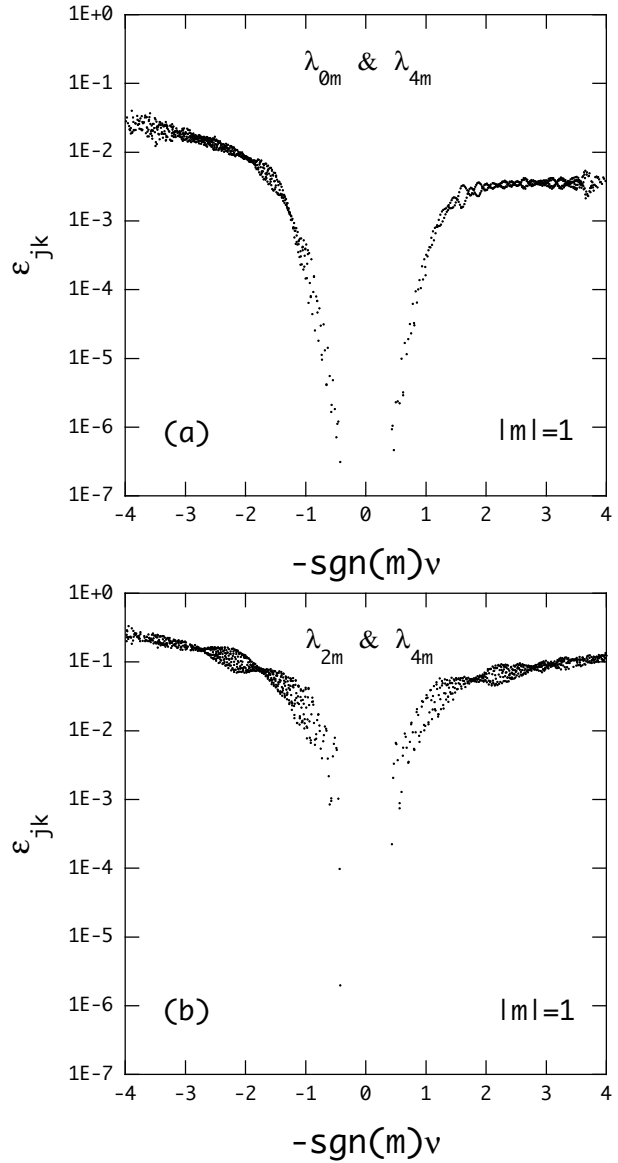


Figure 12. Coupling coefficient ϵ_{jk} between even $|m| = 1$ g -modes associated with λ_{0m} and λ_{4m} in panel (a) and between those associated with λ_{2m} and λ_{4m} in panel (b). Here, we have used the $4M_{\odot}$ ZAMS model, and for $\bar{\Omega} = 0.2$ we have calculated g -modes in the frequency range between $\bar{\omega} = 0.1$ and 1.

The frequency dependence on the rotation frequency can be estimated from equation (12). Since λ_{jm} is proportional to ν^2 for sufficiently large ν (except for prograde sectoral modes with λ_{0m} and $m < 0$), then, ω_R becomes proportional to $\sqrt{2\Omega/n}$ independent of j (or ℓ). Therefore, most of the $\bar{\omega}_R - \bar{\Omega}$ curves become closer to parallel to each other so that broad interactions such as the one shown in Fig. 15 would occur frequently as $\bar{\Omega}$ increases. This explains broad and large peaks of $\bar{\omega}_I$ for tesseral modes with $\ell > |m|$ in the panels (b) and (d) of Fig. 7 and for retrograde sectoral modes with $\ell = m$ with $m > 0$ in the panel (b) of Fig. 8.

The prograde sectoral modes are exceptional. Since λ_{0m} with $m < 0$ is nearly constant for $\nu \gtrsim 1$, they experience only narrow interactions with tesseral modes. This explains why peaks for the prograde sectoral modes seen in the panel

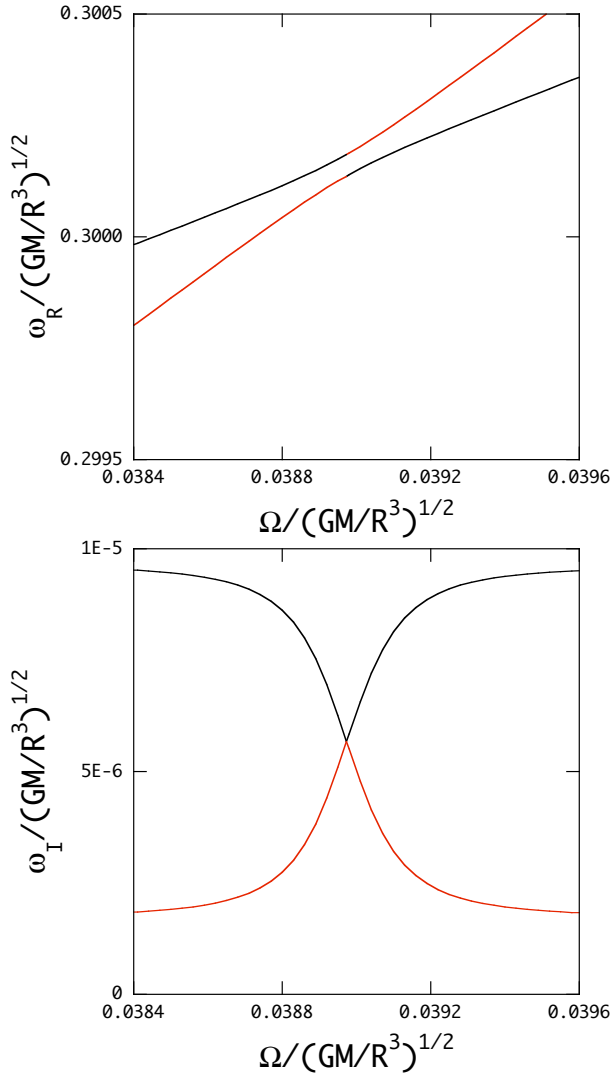


Figure 13. Complex $\bar{\omega}$ of even retrograde ($m=1$) g -modes with $\ell = 1$ and $\ell = 3$ calculated as solutions to the dispersion relation, eq. (13), for the $4M_{\odot}$ ZAMS model. To be compared with Fig. 9.

(a) of Fig. 8 are narrower than those in the other cases. The bumps seen for $\bar{\Omega} \gtrsim 0.2$ can be understood as swarms of numerous weak and narrow interactions.

6 CONCLUSION

We studied the stability of low degree g -modes in uniformly rotating main-sequence stars with masses of $4M_{\odot}$ and $5M_{\odot}$, by taking into account the effects of both the Coriolis force and the centrifugal force, using the method of calculation given by Lee & Baraffe (1995). From the analysis treating $\bar{\Omega}$ as a small parameter we found that a slow rotation has destabilizing (stabilizing) effect on high radial-order retrograde (prograde) g -modes, although the effects for relatively low-order modes are very small or absent. This effect can be understood from the relation between period change due to rotation and the optimal period for the kappa-mechanism at the Fe-opacity bump.

Calculating eigenfrequencies of low degree g -modes at

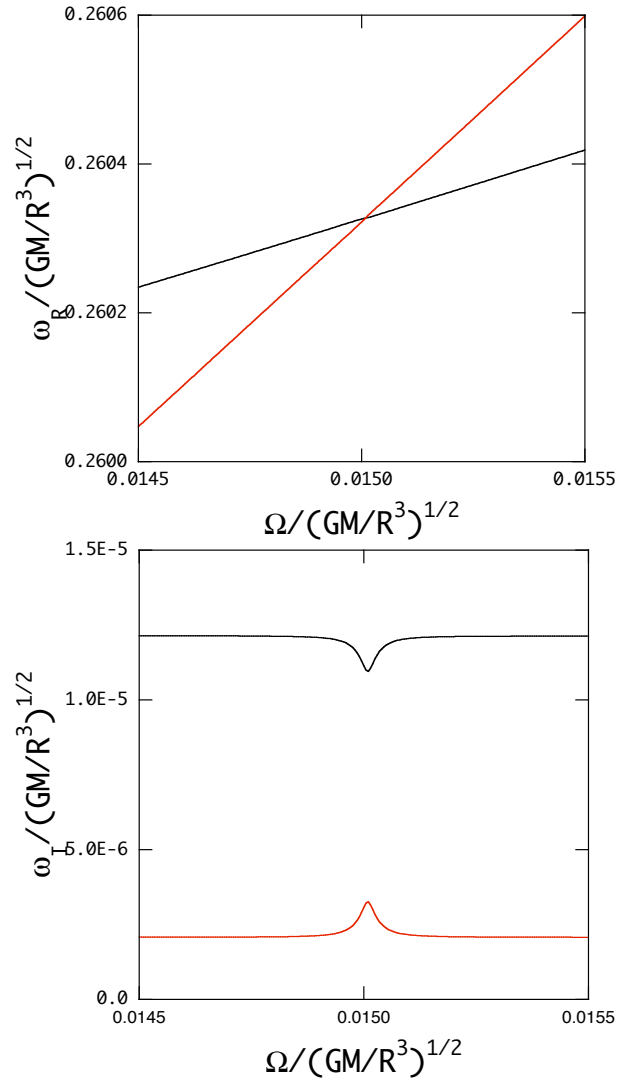


Figure 14. Complex $\bar{\omega}$ of even retrograde ($m=1$) g -modes with $\ell = 1$ and $\ell = 3$ calculated as solutions to the dispersion relation, eq. (13), for the $4M_{\odot}$ ZAMS model. To be compared with Fig. 10.

selected rotation frequencies, we found that, on the other hand, rapid rotation tends to stabilize high radial-order retrograde g -modes, and the stabilizing effect appears stronger for less massive stars with lower effective temperatures.

Obtaining the eigenfrequency of a g -mode of a degree ℓ (associated with a $\lambda_{k\ell}$) as a function of the rotation frequency Ω , we found that it experiences mode crossings with g -modes of different ℓ 's (associated with different $\lambda_{k'\ell'}$'s). At a mode crossing between two modes with the same m and parity (even or odd) a coupling occurs because these two modes are not independent in a rotating star. If an unstable mode crosses a damped mode, the former can be stabilized around the crossing, or vice versa. At a large rotation frequency, low ℓ g -modes, retrograde ones in particular, tend to be stabilized by mode couplings with larger ℓ modes which are strongly damped. The *prograde sectoral* modes ($\ell = -m$ and $m < 0$) in rapidly rotating stars receive exceptionally weak damping effects from mode couplings, because the Ω dependence of their frequencies is very different from the other modes.

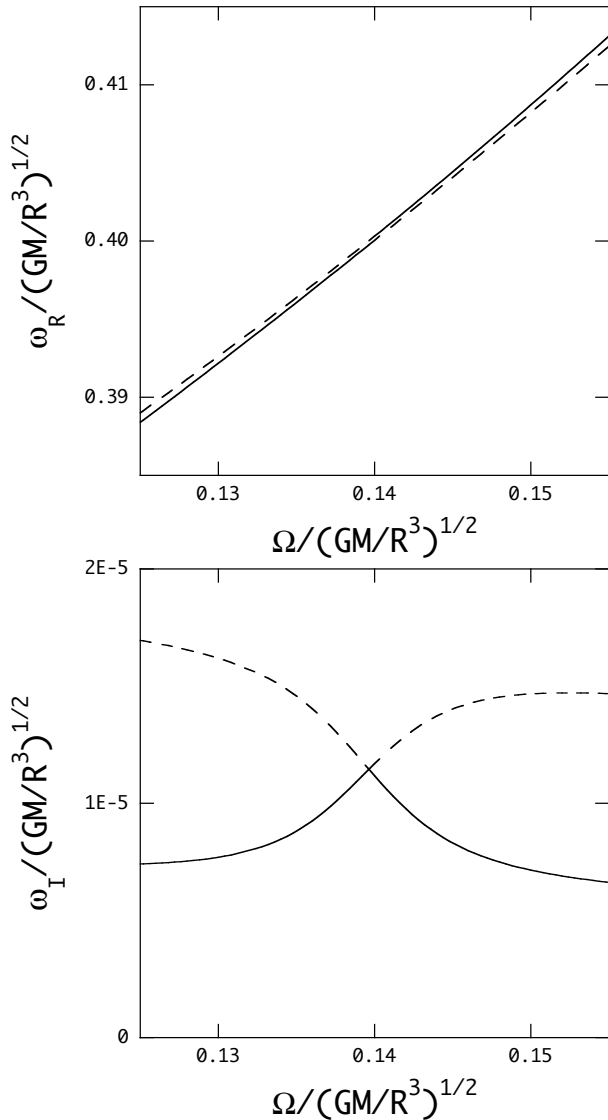


Figure 15. Complex $\bar{\omega}$ of even retrograde ($m=1$) g -modes with $\ell = 3$ (solid line) and $\ell = 5$ (dashed line) calculated as solutions to the dispersion relation for the $4M_{\odot}$ ZAMS model.

We derived a dispersion relation useful to study mode coupling including the radiative damping effect under the quasi-adiabatic approximation. In the dispersion relation the strength of a mode coupling is controlled by a coupling coefficient, ϵ_{jk} between two g -modes belonging to λ_{jm} and λ_{km} ($j > k$); a larger ϵ_{jk} leads to a stronger coupling. The value of ϵ_{jk} is larger when $k \neq 0$ and when $1/\omega_R$ and Ω are larger, and it tends to be larger for retrograde modes than for prograde modes. By using the dispersion relation for various combinations of modes, we could reproduce all types of mode couplings.

To include the effects of the rotational deformation of the equilibrium structure, we employed the Chandrasekhar-Milne (C-M) expansion, where the deformation is assumed to be proportional to $\Omega^2 P_2(\cos \theta)$. This approximation would not be very accurate for a star rotating at a nearly critical rate. One way to avoid the problem would be to employ two-dimensional models, as Ballot et al. (2010) ob-

tained adiabatic g -mode spectrum of two-dimensional rotating polytropes. We hope that it will become possible in the near future to calculate the frequency spectrum and stability for g -modes of two-dimensional evolutionary models.

REFERENCES

- Ballot J., Lignières F., Reese D.R., Rieutord M., 2010, *A&A*, 518, A30
 Cameron C., Saio H., Kushchnig R., et al., 2008, *ApJ*, 685, 489
 Carroll B.W., Hansen C.J., 1982, *ApJ*, 263, 352
 De Cat P. 2007, *CoAst*, 150, 2007
 Dziembowski W.A., Moskalik P., Pamyatnykh A.A., 1993, 265, 588
 Gautschy A., Saio H., 1993, *MNRAS*, 262, 213
 Iglesias C.A., Rogers F.J., 1996, *ApJ*, 464, 943
 Iglesias C.A., Rogers F.J., Wilson B.G., 1992, *ApJ*, 397, 717
 Lee U., 1985, *PASJ*, 37, 261
 Lee U., 2001, *ApJ*, 557, 311
 Lee U., Baraffe I., 1995, *A&A*, 301, 419
 Lee U., Saio H., 1987, *MNRAS*, 224, 513
 Lee U., Saio H., 1989, *MNRAS*, 237, 875
 Lee U., Saio H., 1997, *ApJ*, 491, 839
 Lindzen R.S., Holton J.R., 1968, *J.Atmos. Sci.*, 25, 1095
 Rivinius Th., Baade D., Štefl S. 2003, *A&A*, 411, 229
 Saio H., Cameron C., Kuschnig R., et al, 2007, *ApJ*, 654, 544
 Savonije G.J., 2005, *A&A*. 443, 557
 Shibahashi H., 1979, *PASJ*, 31, 87
 Townsend R.H.D., 2005, *MNRAS*, 360, 465
 Unno W., Osaki, Y., Ando H., Saio H., Shibahashi H., 1989, *Nonradial Oscillations of Stars*, University of Tokyo Press, Tokyo
 Waelkens C., 1991, *A&A*, 246, 453
 Walker G.A.H., Kuschnig R., Matthews J.M., et al, 2005, *ApJ*, 635, L77